ELSEVIER

Computers and Electronics in Agriculture
35 (2002) 111–137

Computers and electronics in agriculture

www.elsevier.com/locate/compag

Insect monitoring radar: stationary-beam operating mode

V.A. Drake *, I.T. Harman, H.K. Wang

School of Physics, The University of New South Wales at the Australian Defence Force Academy, Canberra, ACT 2600, Australia

Abstract

Radars employing the zenith-pointing linear-polarised conical-scan (ZLC) configuration can be adapted to operate in a second mode in which the beam remains stationary and a time-series of echo intensity is recorded as a target traverses the beam. When the targets are insects, the intensity time-series incorporates a slow variation due to the traverse and usually also a modulation that arises from changes in the target's radar cross-section (RCS) due to its wingbeating. A number of target parameters can be retrieved from these time-series: the traverse speed, the wingbeat frequency, the depth of wingbeat modulation and the harmonic content. A lower limit on the target's RCS can also be set. Stationary-beam observations are now incorporated into the operating schedule of two ZLC-configuration insect monitoring radars (IMRs) deployed in inland eastern Australia and datasets of parameter retrievals are routinely produced for several thousand targets per night during periods of heavy migration. This paper describes the stationary-beam mode of IMR operation and presents an analysis of the results for 1 night of heavy migration when Australian plague locusts *Chortoicetes terminifera* are believed to have been the predominant target. Wingbeats were detected for over 68% of the 6631 echoes that were sufficiently strong to be selected for analysis, and strong and quite narrow peaks around 27–31 Hz, as expected for *C. terminifera*, were present in the frequency distributions. Harmonic incidence, modulation depth, target speed and the lower-limit of the RCS were also retrieved with good statistics. Speeds and RCS values were consistent with those from the night's conical-scan observations and, in the case of speed, may be somewhat more reliable. The distributions of most of these quantities varied somewhat with height, in some cases because of range-dependent factors in the radar's performance and in others probably because of differences in environmental conditions and/or the insects' behaviours. The wingbeating parameters all appear to have the potential

* Corresponding author. Fax: +61-2-6268-8786
E-mail address: a.drake@adfa.edu.au (V.A. Drake).

PII: S0168-1699(02)00014-5

for discriminating between targets of different types and the results presented here indicate that an IMR can generate datasets of these parameters that are large enough for reliable inferences to be drawn from them.

Keywords: Radar; Insect migration; Wingbeat frequency; Echo modulation; Harmonic; Radar cross-section; Locust; *Chortoicetes*

1. Introduction

Insect monitoring radars (IMRs) are special-purpose automatically operating radars for quantifying and characterising high-altitude insect migration (Drake, 1993; Reynolds and Riley, 1997). The radar configuration currently being adopted to achieve this function employs a vertical beam and combines linear polarisation with a narrow-angle conical scan (Smith et al., 1993): the ZLC (zenith-pointing linear-polarised conical-scan) configuration[1]. IMRs have been developed to allow long-term monitoring of insect migratory activity, with applications envisaged in research (spatial population ecology), biodiversity monitoring and operational pest management (Drake, 1993; Reynolds and Riley, 1997; Smith et al., 2000; Drake et al., 2001). The primary data products from IMRs are quantitative measures of the intensity and direction of migration and of the variation of these with height and time; these are the outputs that have the potential for incorporation into ecological models, biodiversity indices and pest forecasts. A secondary class of products is concerned with the intrinsic properties of the targets themselves, for example their size and shape; these outputs provide information about the identity of the targets and thus potentially allow more specific interpretation of the primary data. This paper is concerned with a subset of these latter, 'target-characterization', data products: specifically, those acquired by means of a second mode of IMR operation that alternates with the primary, conical-scan observations.

For a radar deployed to monitor insect migration, the primary objective of target characterization is to identify the taxa of the targets that are contributing to the quantitative data products. There is a need to eliminate inanimate targets (e.g. rain and debris items carried aloft in updrafts) and birds and then to classify the insects into categories that are as narrow as possible. Classification to species would allow the greatest utilisation of the quantitative data, but is clearly not achievable, at least in diverse ecosystems, with the relatively limited interrogation capability of radar. A broader categorisation, based around retrievable target parameters, may still provide sufficient discrimination to allow an ecologically informed interpreter to determine whether the quantitative observations relate to the taxa of particular concern. Relating parameter values to taxa could proceed through laboratory or field measurements, e.g. of radar cross-sections (RCSs) and wingbeat frequencies or by examining parameter values retrieved on occasions when species of interest are known to be predominant among the migrants.

[1] Smith et al. (1993, 2000) and Reynolds and Riley (1997) use the term 'nutation' to describe this narrow-angle conical scan and call their radars of this type 'VLR' (for 'vertical-looking radar').

To provide useful information about target identity, a retrieved parameter must represent a property intrinsic to the target and exhibit a range of values that spans and discriminates between a series of taxa. Additional parameters should either span an additional set of taxa or provide independent information about the same taxa, i.e. either extend one dimension in 'identity space' or add an orthogonal one. The intrinsic target parameters that are in principle retrievable from ZLC-radar echoes are size (or mass) and shape (e.g. an estimate of the length/width ratio), the frequency, amplitude and form of any modulations due to wingbeating or other target behaviours, and (though less directly) airspeed. Size, especially if expressed as a mass, appears likely to provide the greatest discrimination: echoes are received from a wide range of target sizes (at least at low altitudes) and the flight-capable (adult) forms of each taxon are confined to a relatively restricted mass range. A study based on laboratory measurements (Aldhous, 1989) has thrown doubt on the utility of shape estimates, but further investigation seems warranted now that IMRs are producing large quantities of field-observation data. Airspeed, retrieval of which has so far not actually been attempted from a vertical-beam entomological radar, is correlated with size in insects (Dudley, 2000) and may therefore provide little additional discrimination, except in respect to distinguishing the largest insects from the smallest birds (which fly much faster) (Schaefer, 1976; Reynolds and Riley, 1997). That wingbeat frequency has some utility for discriminating species has been established in earlier studies (e.g. Schaefer, 1976; Riley and Reynolds, 1979; Drake and Farrow, 1983) with radars that were incapable of providing estimates of target size and it seems sensible to acquire this parameter with the IMRs if this is practicable. The IMR design and operating procedures have therefore been extended to allow the required measurements to be made. Other echo-modulation parameters—the relative intensity of the modulation and of any harmonics that are present and the intensity and frequency difference of any sidebands (attributed by Schaefer (1976) to abdominal respiratory pumping or 'breathing')—may also have value for discriminating between target types. An initial research objective will be to assess whether the availability of these types of target-characterization information significantly enhances an IMR's capacity for identifying the targets it detects.

Unfortunately, in the usual ZLC-mode of operation, the intrinsic echo modulations are swamped by the much larger variations in echo intensity produced by the conical scan. A second mode of operation, in which the beam remains stationary, has therefore been incorporated into the observation procedure. This has two undesirable consequences: first, echo modulations cannot be retrieved for the same individual targets that size, shape and airspeed estimates are obtained for, as these latter parameters all derive from conical-scan data; and secondly, the time available for acquiring the primary quantitative data products is reduced. However, some compensation for the loss of ZLC observations may be possible, as a range of information can be extracted from the stationary-beam data. In addition to the wingbeat frequency, several other parameters characterising the intrinsic modulation can be estimated, along with the target's speed and a lower limit on its RCS.

This paper describes the acquisition and analysis procedures employed in the stationary-beam mode of IMR operation and presents some typical results. The

data come from an IMR located at Bourke, New South Wales (30°2′ S, 145°57′ E), in eastern inland Australia, and were obtained in February 1999, i.e. summer, during a period when Australian plague locusts *Chortoicetes terminifera* were known to be numerous in the region. Some associated theory is presented in Appendix A.

2. The stationary-beam operating mode

The ZLC configuration employs a nearly vertical beam, so in all observation modes the target is interrogated from almost directly below as it flies overhead. The beam offset required for the primary conical-scan operating mode (Smith et al., 1993; Fig. 1a) is still present when the beam is stationary, but the deviation from vertical is so small (0.2°) that its effect can be assumed to be negligible. A vertical beam has the advantage for target-characterization purposes that, provided the insects maintain a horizontal and upright orientation, the beam is consistently aligned at right angles to their body axis and through their plane of symmetry.

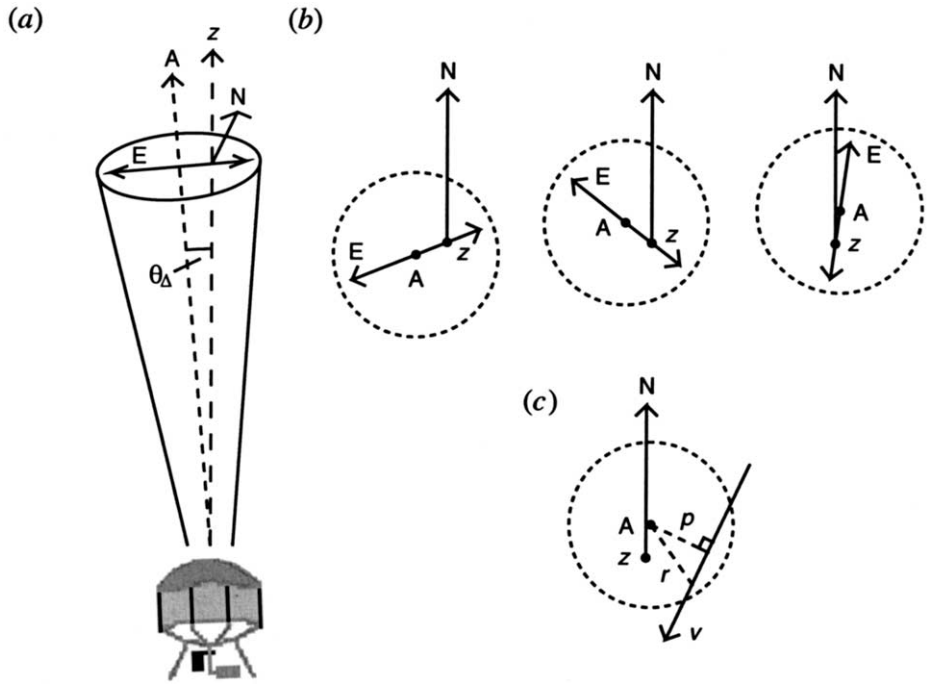

Fig. 1. (a) Geometry of IMR beam, showing offset θ_{Δ} from vertical required for conical-scan operation (angles exaggerated). (b) Set of three polarization alignments used for stationary-beam observations by the Bourke IMR. (c) Traverse of target at speed v and distance of closest approach p; r is the instantaneous distance from the beam axis. Key: A, beam axis; E, polarization (alignment of electric field); N, north; z, axis of antenna rotation (aligned with zenith).

Observing at a significant slant angle would add additional, extrinsic, potential sources of variation in the modulation intensity that would make it harder to extract the required information. There have also been indications, from observations with earlier types of entomological radar (Drake, unpublished data; J.R. Riley, personal communication), that wingbeats are more readily detectable (i.e. produce a larger modulation intensity) when the beam is vertical than when it is directed at slanting angles.

A vertical beam does not eliminate all potential biases, however: because the beam is linearly polarised, there will be large variations in echo amplitude depending on how the target is aligned relative to the electric field (Riley and Reynolds, 1979). If the targets were oriented at random, this would not be a great concern as some would be aligned nearly parallel to the polarisation (and thus produce an echo that is strong enough to be detected and analysed) and these would be representative of the population as a whole. However, targets frequently exhibit collective orientation (e.g. Riley and Reynolds, 1979; Drake, 1983) and observations at more than one polarisation angle are required to ensure a representative sample of echoes is obtained. In the current IMR design, this is achieved by making observations at a sequence of three polarisation angles 60° apart (Fig. 1b). If collective orientation is present, its direction will be within 30° of the polarisation angle for one of the three samples and available RCS data (Riley, 1985; Aldhous, 1989) suggests that, for most species, the echo amplitude will then be within ~ 2 dB of the maximum possible.

The Bourke IMR operates on an hourly cycle which commences on the hour with a sequence of conical-scan observations lasting ~ 17 min. The radar then switches to stationary-beam observing mode for ~ 10 min before recommencing conical scanning for a second ~ 17-min period. A period of idling and a self-test and performance-optimisation procedure complete the cycle. Target-characterisation data are thus acquired hourly and can be related to both the immediately preceding and the immediately following set of quantitative observations. The three data-acquisition periods in a stationary-beam sequence each last 157 s and are separated by intervals of ~ 1 min during which the antenna feed is automatically aligned to the next polarisation angle.

Observations are made with a nominal pulse duration of 50 ns and a pulse repetition frequency (PRF) of 2500 Hz. The transmitter is triggered by a pulse train generated on a counter-timer card (PCL-830, Advantech Co., Taiwan) within the control microcomputer (Figs. 2 and 3). (This trigger signal replaces that used during conical-scan observations, when the trigger is generated from a shaft encoder on the rotating-feed assembly.) A conditioning circuit converts the trigger signal to the form required by the transmitter. The echo signal from the antenna passes through the normal receiver, distribution-amplifier and gated peak-hold circuitry (Fig. 2) and therefore is subjected to logarithmic amplification (which accommodates a wide range of echo intensities). The Bourke IMR has eight gates, each 333-ns wide, spaced at 1000-ns intervals; these values correspond to 50 m for the sampling-interval depth and 150 m for

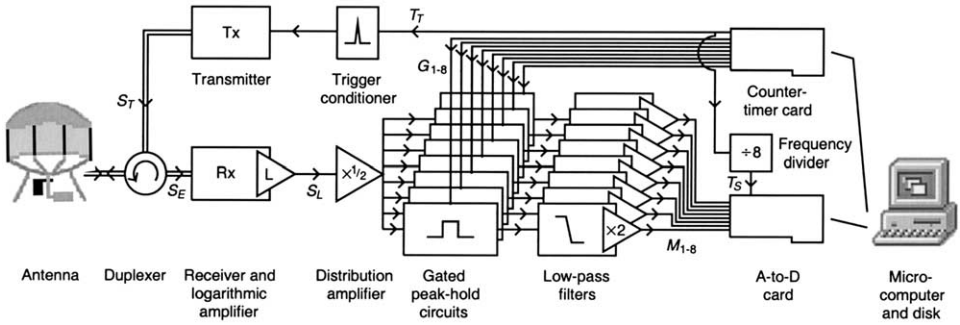

Fig. 2. Block diagram of IMR stationary-beam triggering and signal-acquisition system (eight-parallel version). Key: Tx, transmitter; Rx, receiver; T_T, transmit trigger; T_S, sampling trigger; S_T, transmitted pulse; S_E, echo signal; S_L, detected and log-transformed echo signal; G_{1-8}, gates 1–8; M_{1-8}, echo-modulation signals from gates 1–8. [Microcomputer graphic courtesy of 'Iconolog' (http://www.iconolog.net/)].

the spacing. The bottom-most sampling interval starts at 200 m (because the performance of the radar's receiver is degraded at shorter ranges than this) and the top-most extends to 1400 m. Only one-third of the 200–1400 m observing range is sampled: continuous coverage could be effected by moving the gates (as is carried out during conical-scan observations) and taking more (possibly shorter) samples, but this has not been considered warranted.

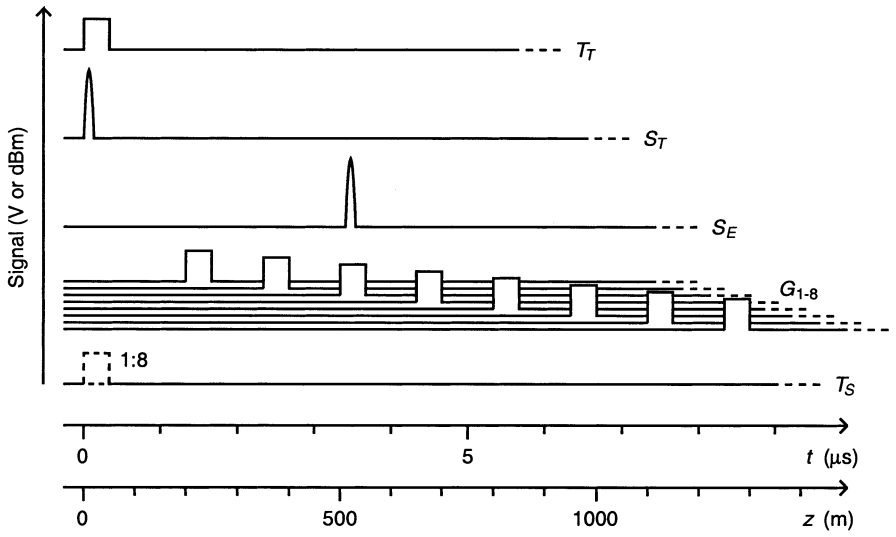

Fig. 3. Sequence of signals in IMR stationary-beam triggering and signal-acquisition system (eight-parallel version). See Fig. 2 for key. The sampling trigger fires only once every eight cycles.

The outputs from the peak-hold circuits range between 0 and 4 V, with 1 V corresponding to a change in echo-intensity of ~ 20 dB. These outputs are fed into a bank of low-pass filters (Sallen-Key sixth-order active filters, Butterworth characteristic, cut-off frequency 128 Hz) (Simpson, 1987) to eliminate any higher frequencies that might cause aliasing and then digitised to 12-bit precision (range: 0–4096, representing -5 to 5 V, step size ~ 2.4 mV) at a frequency of 312.5 Hz. Scaling of the signal is incorporated where necessary to ensure it fits within, and makes full use of, the working ranges of the various circuits. The sampling trigger is derived from the transmit trigger by a frequency divider ($\div 8$) circuit. The sampling and low-pass filter frequencies were selected to allow detection of wingbeats up to ~ 100 Hz and also for compatibility of the circuitry with conical-scan operation (for which the sampling frequency is 320 Hz). Filtering effectively averages the signal, so that the 312.5 Hz samples have a much better signal-to-noise ratio than the 2500 Hz peak-hold outputs.

Data from each 157-s acquisition period is written to disk as a single, multiplexed, binary file of 768 kbyte. The time of acquisition and the automatically generated unique filename are appended to the radar log file for the night. The log file serves as an index to the observations and is used by the automatic data-analysis procedures to control processing of the files (Drake et al., 2002). It also contains outputs from the radar's self-test and performance-monitoring procedures and these are inspected periodically for any indications of deteriorating performance.

Stationary-beam observations, including stopping and polarisation-realignment time, occupy ~ 11 min in each hour (18% of available time) in comparison with the 33 min (55%) occupied by conical-scan observations.

3. Stationary-beam signals

At low densities ($< \sim 10^{-3}$ m^{-3} at 200 m, $< \sim 2 \times 10^{-5}$ m^{-3} at 1400 m), individual targets are usually sufficiently separated for them to appear as discrete echoes that are readily identifiable in the recorded signal (Fig. 4a). In the 30-s section shown in the figure, three echoes are evident at the higher altitude and ~ 25 at 200–250 m, with some of the latter overlapping. The steady (usually windborne) traverse of the targets across the Gaussian beamshape (Fig. 1c) produces, after logarithmic amplification, an approximately parabolic signal shape (Fig. 4(b) and see Appendix A for a mathematical treatment.) The width of the parabola is determined by both the altitude and the speed of the target (Eq. (A11)), while its height results from both the size of the target and its distance of closest approach to the beam axis (Eq. (A7)). The latter cannot be determined from these observations, so the parabola's height provides only a lower limit on the target RCS, this being calculated on the assumption the target's traverse intersected the axis of the beam. Superimposed on the parabola are some random fluctuations arising from system noise (r.m.s. ~ 0.3 dB) and in the majority of our examples, a small-amplitude (typically between 0.5 and 1.5

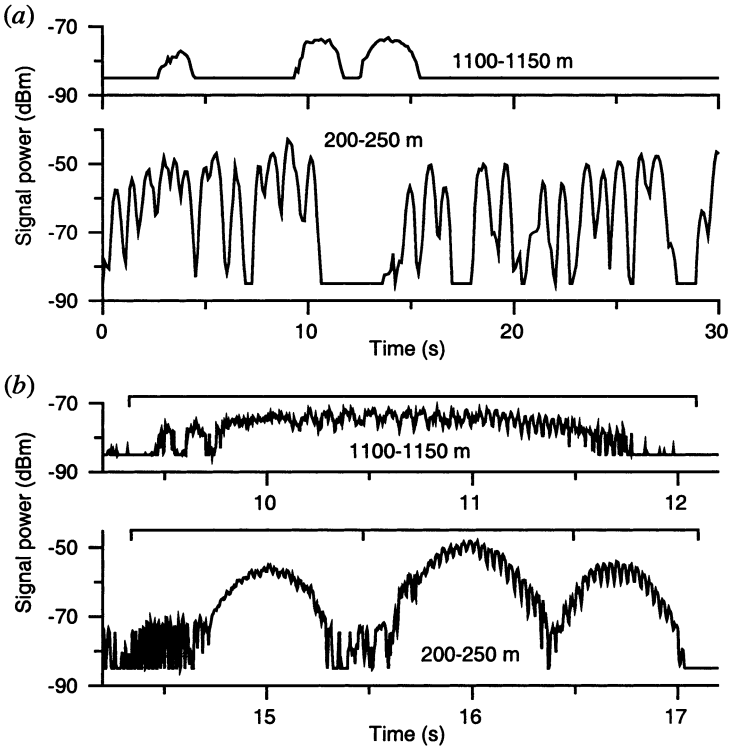

Fig. 4. (a) Sections of digitised signals, averaged over 32-point (~ 0.1 s) sequences, from the Bourke IMR at 20:32 h on 11 February, 1999. Top, gate at 7.33–7.67 μs, covering heights from 1100–1150 m; bottom, gate at 1.33–1.67 μs, covering heights from 200–250 m. (b) Expansions of portions of the sections in (a); the selections made by the initial stage of the echo identification and delimiting algorithm are also indicated.

dB) modulation arising from wingbeating and possibly other target behaviours. Because of the logarithmic transformation in the receiver, the magnitude of the modulation in the digitised sequence is a 'relative' measure of the intensity of the modulation in the echo, i.e. it indicates the size of the modulation as a proportion of the total power returned from the target. The digitisation step size (2.44 mV, $\equiv \sim 0.05$ dB) sets a lower limit on the magnitude of the modulation that will be detectable.

At higher densities ($> \sim 10^{-3}$ m^{-3} at 200 m, $> \sim 2 \times 10^{-5}$ m^{-3} at 1400 m), echoes overlap. Strong modulations due to interference will arise if more than one target is present within a pulse volume (Schaefer, 1968). Interference effects completely obscure the much smaller modulations due to wingbeating and little if any target-characterization information can be retrieved. Such echoes are a potential source of contamination if not identified and rejected. When interference arises from insects that are much smaller (but perhaps more numerous) than the species being investigated, the effect will be like an additional source of noise that will degrade any wingbeat modulation but not necessarily obscure it entirely.

4. Parameter retrieval

The digitised signal voltages are first converted to logarithmic-transformed power (dBm) values using a characteristic curve obtained from laboratory calibrations of the receiver and the gated peak-hold circuits. A preliminary algorithm then identifies and delimits echoes from discrete targets, i.e. peaks in the signal that rise significantly above the background noise level. The dBm values are first averaged over intervals of 32 points (~ 0.1 s), to smooth out the most rapid fluctuations (including those due to wingbeating) and to reduce the signal dataset to a tractable length (1536 points at each of the eight heights). Echoes are selected if the smoothed signal rises at least 8 dB above its background noise level and are initially delimited at the points where it falls to 2 dB above background, or at the first minimum of depth 1.5 dB or more that is encountered, or after 5.12 s (1600 points). Selections that are < 0.4 s long are discarded. These initial selections, which are non-overlapping, are then truncated at both ends, at the points where the smoothed signal falls 6 dB below its value at the peak; any selections that are reduced to < 48 points (~ 0.15 s) by this process are discarded. Very long signals are further truncated symmetrically around the peak to reduce them to a maximum length of 1024 points (~ 3.3 s).

Parameter retrieval proceeds by fitting a parabola (Eq. (A10)) to the truncated signal, using a least-squares algorithm which incorporates weighting of each point (by the inverse square of the estimated error on the logarithmic power) and single-value decomposition (Nash, 1979; Press et al., 1993). Signals are rejected if the fitted parabola is inverted (a_f in Eq. (A10) positive rather than negative) or if its maximum falls outside the selection interval, or if the uncorrected R^2 coefficient for the fit (Nash, 1979) is < 0.5. The R^2 cut-off was set following inspection of the graphical output from a small sample of signal analyses and is intended to eliminate fits to inappropriate signal selections without excluding signals showing strong wingbeat modulations. The speed of the target through the beam is then estimated from the quadratic term in the parabola and the radar beamwidth (Eq. (A11)) and the precision of this speed estimate is calculated from the uncertainty on the quadratic term (Eq. (A12)). The lower limit on the RCS is calculated from the parabola's peak value (Eq. (A14)) and the radar's sensitivity (Eq. (A15)). (This value also incorporates a scaling factor introduced to overcome discrepancies between our field estimates of the size of overflying *C. terminifera* and those measured by Schaefer (1976) in more controlled conditions; the need for this scaling presumably indicates deficiencies in our radar calibration procedure or a subsequent deterioration of radar performance.) All results, together with goodness of fit parameters and the height at which the echo was acquired, are included in a record for the echo that is subsequently written to the results (or FIT) file (Drake et al., 2002) for the night.

The fitted parabola is then subtracted from the truncated signal (Eq. (A26)) and the residual transformed exponentially (Eq. (A27)) to produce a new signal that is proportional to the 'voltage modulation factor', i.e. to the square root of the modulation of the echo power. The mean of this signal is calculated and subtracted

and a window function (Eq. (A28); Lyons, 1998a) applied to it. The windowed signal is zero-padded at the tail (Lyons, 1998b) to exactly 2^N points ($6 \leq N \leq 10$, thus minimum 64 and maximum 1024 points) and analysed by a fast Fourier transform (FFT) algorithm (Press et al., 1993). The power spectrum is then calculated from the real and complex components of the FFT and scaled for the effects of windowing and zero-padding (Eq. (A30) and Eq. (A31)). A point on this spectrum represents the power of the modulation at the particular frequency as a proportion of the peak power of the echo. The analysis process is illustrated for two typical echoes in Fig. 5. Analysis stages are: parabolic fit (shown displaced upwards from the original signal by 10 dB); subtraction of parabola and antilogarithmic transformation to a 'voltage' modulation; application of window and zero-padding; FFT calculation of periodogram (shown at bottom); and automatic identification of spectrum features. The wingbeat modulation is obvious in the signal in (a), but in (b) is obscured in places by lower-frequency modulations that probably arose from interference from a second, nearby, target. The maximum analysable frequency (the Nyquist critical frequency, f_c) is half the sampling rate, i.e. ~ 156 Hz and the frequency bin size is $f_c/2^{N-1}$, which varies between ~ 5 Hz for the shortest and ~ 0.3 Hz for the longest echoes.

The final stage of the analysis is the identification of fundamental and harmonic peaks in the power spectrum. The section of the spectrum corresponding to frequencies of 14 Hz or less is excluded, as few insects beat their wings this slowly and the significant power that is sometimes observed in this range presumably arises from other processes (e.g. orientation changes, perhaps associated with encounters with turbulent eddies). An average power (shown as a horizontal dashed line in Fig. 5) is calculated for the whole spectrum (0–156 Hz), and the fundamental identified as the strongest peak that is at least $8\times$ higher than this. The width of the

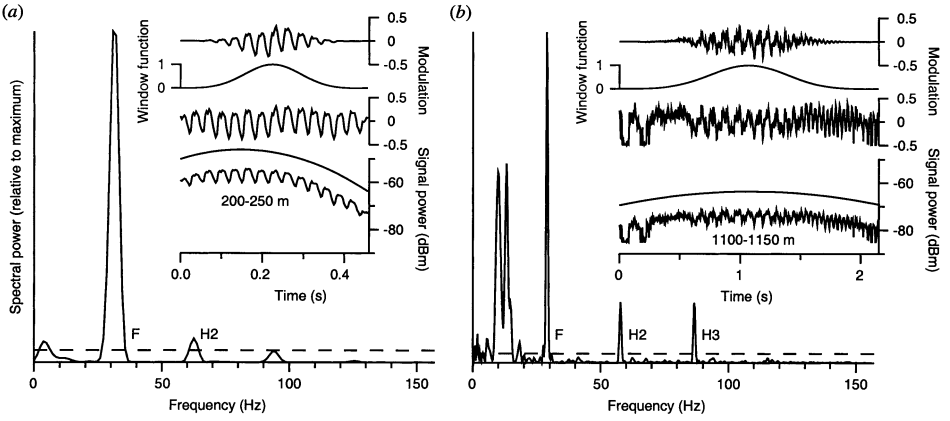

Fig. 5. Analysis of two of the echoes in Fig. 4(b), after second-stage delimiting. (a) Echo from 16.5 to 17.1 s at 200–250 m, 144 points; (b) echo from 9.3 to 12.1 s at 1100–1150 m, 672 points. See text for explanation of analysis stages. Automatically identified features are marked by codes as follows: *F*, fundamental frequency; *H*2, second harmonic; *H*3, third harmonic.

fundamental is determined by the first minimum on either side of the peak and its power estimated as the sum of the powers for all the bins between (and including) these minima. The fundamental is accepted if this power exceeds 10% of the total power of the spectrum. Its frequency is estimated from the powers of the peak and its two neighbours by a quadratic interpolation (Eq. (A33)). Harmonics are then identified as peaks that fall within a narrow range (seven bins wide) of the expected frequency multiples and that reach at least $1.5\times$ the average power level. Widths, frequencies and powers for the harmonics are calculated as for the fundamental. The automatically identified features of the power spectra of Fig. 5 are indicated in the figure. The outputs of the analysis—the frequencies and relative powers of the fundamental and any detected harmonics—are appended to the record for the echo in the FIT file.

These analyses are made with purpose-developed programs written in the C++ language (Stroustrup, 1991) and running on microcomputers with '486' or 'Pentium' CPUs. Analysis takes place on the IMR's control microcomputer, during the morning following the night on which the data were acquired; analysis can also be carried out offline, from data archived on CD. The data-processing and results-dissemination systems are described more fully by Drake et al. (2002). Stationary-beam raw-data files contribute 20% of the raw-data disk-space requirement of ~ 130 Mbyte each night. For the night of 11–12 February 1999 (see Section 5), they produced 4582 records (23% of the total) with one or more estimated parameters, in comparison with 15665 (77%) records with equivalent content from the conical-scan data.

5. Some typical results

In this section, a summary of the results for the night of 11–12 February, 1999 is presented. This was a night of heavy migration, which the conical-scan observations showed to be predominantly of *C. terminifera*-sized insects moving to the WNW and aligned mainly along a NNW/SSE axis. Observations continued for 8 h, from 19:00 to 02:40 h LST, and over this period there were only minor variations in migration direction, speed and alignment and in target size. In this summary, data from all periods of the night have generally been combined, but variations with altitude are presented explicitly because the changes in beamwidth and radar sensitivity with height will introduce some systematic variations in the distributions of echo characters.

The variations with height and time of the number of selected signals are shown in Fig. 6(a,b). The unshaded portions of the histogram bars represent signals that were truncated during the selection process to <48 points, signals for which a good-quality parabolic fit was not achieved and signals in which no fundamental frequency was detected. A fundamental was identified in 68% of the signals and in all but 1% of the signals that gave good-quality parabolic fits; 58% of the fundamentals were accompanied by at least one harmonic. The different numbers of echoes at different heights and times can be attributed principally to the

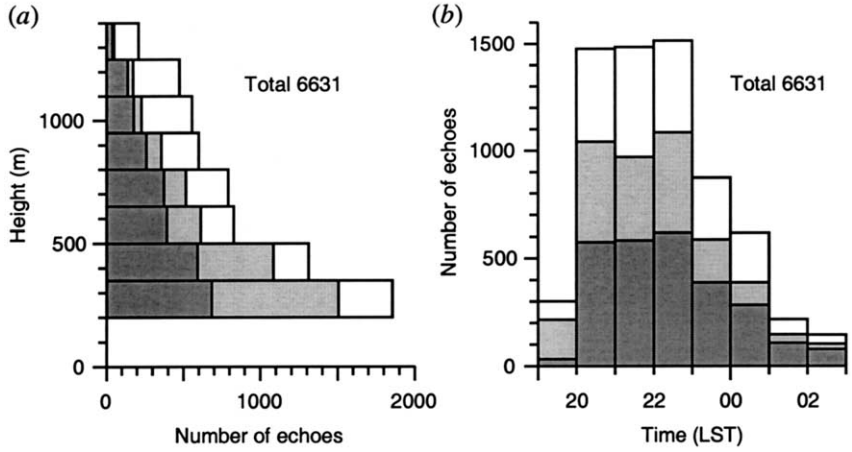

Fig. 6. The variations with (a) height and (b) time of the number of signals selected during the night of 11–12 February, 1999. The shaded portion indicates the number of these with a fundamental identified and the dark shading the number for which one or more harmonics were also detected.

behaviour of the insect targets. The incidence of harmonics is discussed further below.

The distributions of signal selection lengths (both initially and after truncation) and the proportions for each length of analyses in which a fundamental frequency was detected are shown in Fig. 7. As is to be expected, durations are longer at higher altitudes where the beam is broader. Some signals acquired in the highest gates have evidently been truncated to the maximum signal lengths in both the initial and the second delimiting stages. A lower rate of detection of fundamentals at higher altitudes (Fig. 7a) is due to signals overlapping there and failing to make good-quality parabolic fits, a consequence of the relatively high target density on this occasion. The distributions also indicate, unsurprisingly, that at similar heights (i.e. similar signal-to-noise ratios), a longer signal is more likely to result in a good-quality fit, and thus to reveal a fundamental, than a shorter one.

Distributions of the speeds estimated from the parabolic fits, and of the precisions of these estimates, are shown in Fig. 8. Speeds were retrieved from 69% of the selected signals. They are concentrated into rather broad peaks (full width at half maximum ~ 6 m s^{-1}) at between 7 and 11 m s^{-1}; these appear consistent with windborne transport possibly supplemented by an airspeed contribution of ~ 4 m s^{-1} (Drake et al., 2001) for the larger targets. The decrease of speed with height evident on this occasion can be tentatively attributed to a wind profile of the low-level jet type (Drake and Farrow, 1988). The precisions of the speed estimates are mostly better than 0.3 m s^{-1}, although there is a long upper tail. The precision varies little with height, with the greater signal lengths at high altitude presumably compensating for the shallower parabola that results from the much greater beamwidth there. Typical precisions are much less than the spread of speeds observed, suggesting that this spread is real and that stationary-beam observations may be capable of resolving its component contributions.

The estimates of the lower limit of the RCS are shown in Fig. 9. A broad peak centred around 0.6 cm^2 is evident at all heights (Fig. 9a), with a range of smaller values also present at the lower altitudes. Detection thresholds (incorporating the requirement that the echo rises at least 8 dB above the background noise level) of ~ 0.011 cm^2 at 500 m and ~ 0.14 cm^2 at 950 m account for the lack of smaller values in the upper two graphs. For the 200–500 m results, distributions are shown for each of the three beam-polarisation angles in Fig. 9(b). A shift in the location of the peaks is evident, with the echoes strongest when the polarisation was aligned to 304°, i.e. closest to the $\sim 315°$ mutual-alignment direction of the targets in this height range, as determined from the conical-scan observations. The peak at polarisation angle 304° was located at 0.8 cm^2, while those for 004° and 244° were at 0.4 and 0.2 cm^2, respectively, i.e. reduced by factors of 3–5 dB. The slightly higher position of the 004° peak, compared with that at 244°, is consistent with the $\sim 315°$ alignment from the conical scan.

The presence of a peak in these distributions suggests targets of a relatively narrow size range were predominant in the overflying population. The spread of values on the low side of the peak qualitatively resembles the distribution expected from off-axis traverses (Eq. (A22); Fig. 13), that will tend to smear the peak towards lower values. However, it is likely some smaller targets were also contributing, at least at lower altitudes and especially around 0.005 cm^2, where counts seem

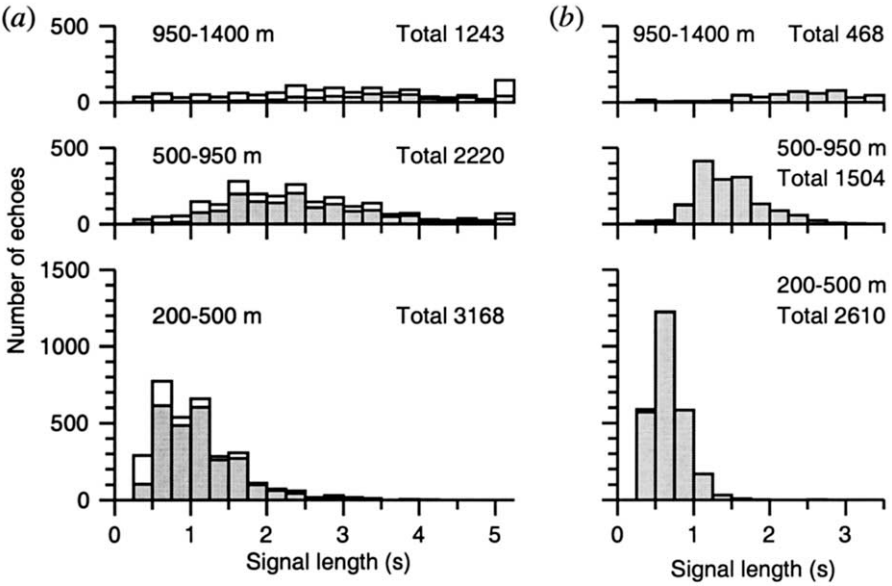

Fig. 7. Distributions of signal selection lengths, partitioned into low (200–250 m, two gates), medium (500–950 m, three gates) and high (950–1400 m, three gates) altitude ranges, for the night of 11–12 February, 1999. (a) Initial selection; (b) truncated selection as subjected to parabolic fit and spectral analysis. Selections for which a fundamental frequency was detected are shown shaded. Only echoes for which the quality of the parabolic fit was good are included in (b).

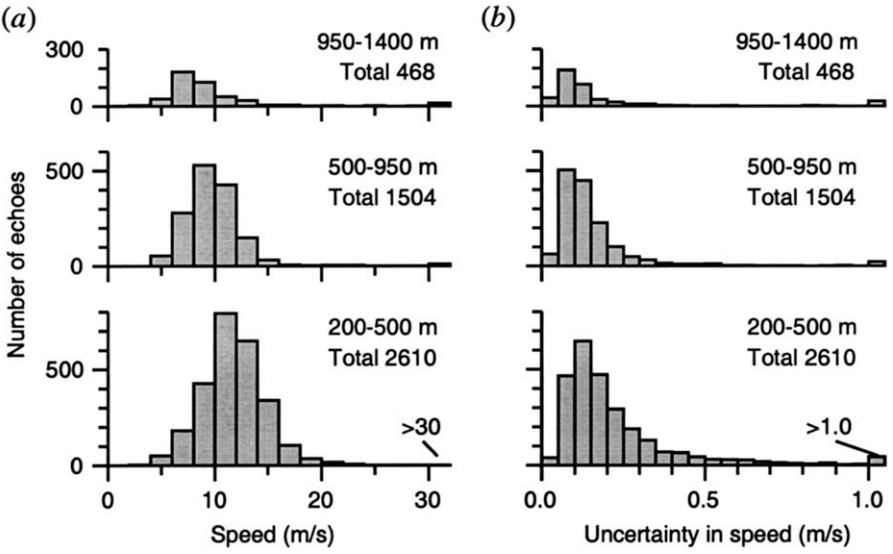

Fig. 8. Distributions of (a) estimated speeds and (b) uncertainties in the speed estimates, partitioned by altitude as in Fig. 7, for the night of 11–12 February, 1999.

to rise above the general trend. There is little indication of the predominant size varying with altitude. The range of actual RCS values can perhaps be inferred from the spread of values above the peak in the observed distribution. For the polarisation angle 304°, where the peak is at the highest RCS value, this region corresponds well with the range of maximum RCS (σ_{xx}) values estimated from the conical-scan observations (Fig. 9b).

The results of the spectral analyses of the signals are shown in Figs. 10–12. Fundamental frequencies (Fig. 10a) are concentrated into a quite narrow band, the centre frequency of which decreases from 31 Hz at altitudes below 500 m to 27 Hz above 950 m. The full width at half maximum for the peak is ~ 6 Hz at all altitudes. Modulations at other frequencies, especially in the range 12–25 Hz, are also present. The 27–31 Hz range is consistent with measurements of *C. terminifera* wingbeating under experimental conditions (summarised in Drake and Farrow, 1983), when frequencies were in the range 26–33 Hz. A decrease of frequency with height was detected also in the similar-sized acridid *Aiolopus simulatrix* in Africa (Schaefer, 1976) and probably results from a decrease of air temperature with height; lower values, centred around 23 Hz, observed during nocturnal *C. terminifera* migration over central-western New South Wales (Drake and Farrow, 1983) may also reflect cooler conditions. The intensities of the relative modulations peak around 5×10^{-2} (Fig. 10b), corresponding to an RCS modulation of ~ 0.6 dB or $\sim 15\%$. These distributions are broad, with half-maximum ranges spanning approximately a decade, but vary little with altitude.

The incidence of harmonics is shown in Fig. 11. For a fundamental frequency of 30 Hz, up to four harmonics can be present below the 156-Hz upper limit of the analysis. The number of echoes for which two harmonics were detected is almost equal to the number for which only one was found (Fig. 11a). The majority of the detections are of second and third harmonics, with the former significantly outnumbering the latter (Fig. 11b). The proportions of echoes for which different combinations of these two harmonics are found (Fig. 11c) may provide the most satisfactory characterization of the incidence of harmonics in an echo sample. All the Fig. 11 distributions and Fig. 6(a) indicate that the capacity for detecting accompanying harmonics increases with altitude. This is tentatively attributed to the longer signals there (Fig. 7) allowing improved discrimination of weak spectral components from noise, even though the signal-to-noise ratio of the echoes from these relatively distant targets will be less than that for echoes from targets closer to the ground. The variation with time evident in Fig. 6(b) can be attributed to similar signal-length effects, as targets were largely confined to low altitudes early in the night, but were present predominantly at high altitudes after midnight.

The distributions of the intensities of the second and third harmonics relative to the fundamental are shown in Fig. 12(a,b) and, for echoes where both are present, the distributions of the intensity of the third harmonic relative to the

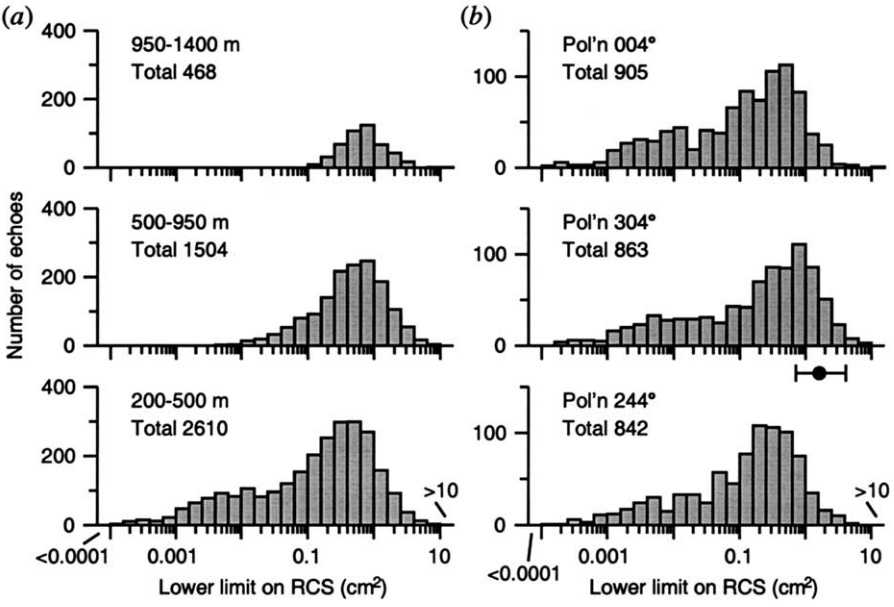

Fig. 9. Distributions of the estimates of the lower limit on the RCS, partitioned in (a) by altitude as in Fig. 7 and in (b) by beam polarization direction (see Fig. 1b), for the night of 11–12 February, 1999. Only echoes in the bottom two gates (200–500 m altitude range) are included in (b). The peak value (1.6 cm^2) and width (to half maximum) of the distribution of maximum (σ_{xx}) RCS values estimated from the conical-scan observations for the same night are shown below the 304° histogram.

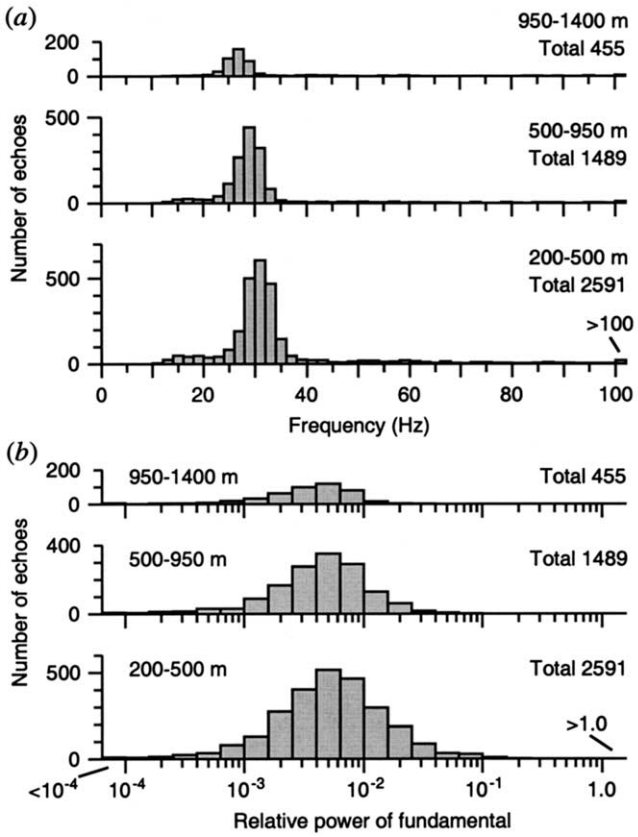

Fig. 10. Distributions of (a) the detected fundamental frequency of the modulation and (b) the power of this fundamental modulation relative to that of the whole echo, partitioned by altitude as in Fig. 7. Results are for the night of 11–12 February, 1999.

second are shown in Fig. 12(c). Second-harmonic power is typically 10–20% of the power of the fundamental and the third harmonic, if present, is typically 1.5–2 × stronger than the second. These trends show little variation with height.

Sideband peaks on either side of the fundamental, as reported by Schaefer (1976) for desert locusts *Schistocerca gregaria*, have not been found in this dataset. Artefactual sidebands commonly appear, as a result of leakage, when Fourier analysis is carried out on finite-length signals that do not smoothly approach zero at each end (Lyons, 1998a) and they can be made to appear in our spectra by omitting application of a window. Possibly, sidebands will be detectable in IMR echoes from larger targets such as *S. gregaria* or, in Australia, the spur-throated locust *Austracris guttulosa*. However, our current analysis system does not attempt to identify them or to record their parameters.

6. Discussion

The results presented here show that an IMR observing in the stationary-beam mode can produce large samples of estimates of a number of characters of the overflying targets. The high success rate (almost 70%) of the analyses of individual echoes leads to the accumulation of significant statistics (thousands of data points on a 'heavy' night, Figs. 6–12) from a moderate allocation (11 min in each hour) of observing time. This time could, nevertheless, be allocated to conical-scan observations, to produce not just larger samples of the quantities obtainable from these but also to provide greater continuity of coverage (e.g. 15 min rather than 30 min time resolution). Whether inclusion of stationary-beam operation in the observing cycle produces a net benefit will be determined primarily by the interpretative value of the various parameters describing the targets' wingbeat modulations, as these cannot be obtained by other means. Retrieval of target numbers and speeds, and of the lower limit on the RCS, will essentially duplicate information that will be available anyway from the conical-scan observations. The two observation methods can be expected to exhibit different efficiencies and biases, however, and the relative simplicity of the stationary-beam data may therefore confer

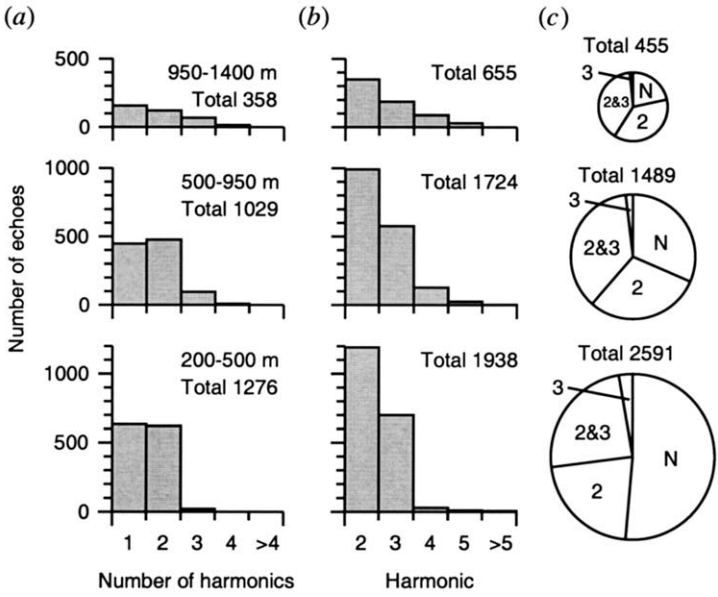

Fig. 11. Distributions of (a) the number of harmonics detected in each signal; (b) the numbers of each harmonic detected and (c) the proportion of signals for which various combinations of the second and third harmonics were detected. Results are for the night of 11–12 February, 1999 and are partitioned by altitude as in Fig. 7. Key: *N*, fundamental detected but neither second or third harmonic found; *2*, fundamental and second harmonic detected but third harmonic not found; *2 & 3*, fundamental and both second and third harmonics all detected; *3*, fundamental and third harmonic detected but second harmonic not found.

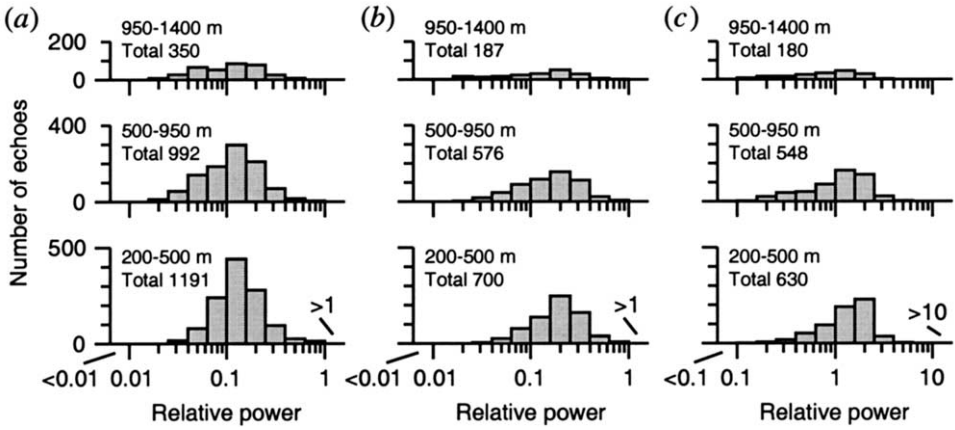

Fig. 12. Distributions of the power relative to the fundamental of (a) the second and (b) the third harmonics. (c) Distribution of the power of the third harmonic relative to the second. Results are for the night of 11–12 February, 1999 and are partitioned by altitude as in Fig. 7.

advantages; also, at high densities, the absence of a scan will marginally reduce the incidence of interference from nearby targets. For these reasons, the utility of the estimates of each of the parameters retrievable from stationary-beam observations deserves evaluation. Abandoning the conical scan altogether, which would significantly simplify the radar design, is not an option because no information would then be available on a key migration parameter, the direction of movement.

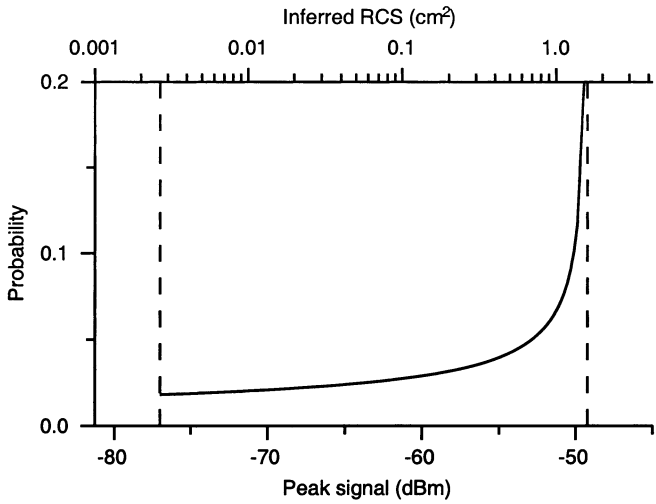

Fig. 13. Distribution of echo powers predicted from Eq. (A22). The particular curve drawn is for targets with radar cross-section 1.6 cm^2 passing over the Bourke IMR at an altitude of 350 m, i.e. approximately as in the distributions of Fig. 9(b). Radar parameters used are $s_{thr} = -77$ dBm and $s_0 = -65.5$ dBm (when $\sigma = 1$ cm^2 and $R = 1$ km). The upper scale shows the RCS that would be inferred by assuming that the target passed through the beam axis.

Only a limited assessment of parameter utility is possible with the single-night dataset presented here. The forms of the distributions in Figs. 7–11 have some implications for potential diagnostic value, or discriminating power, of the various retrieved parameters and these will be discussed. A more complete assessment might compare distributions from several nights, including some when taxa other than *C. terminifera* are likely to have been predominant. It would also need to examine how much extra diagnostic power is provided over that of the target-characterization parameters (principally size and shape) available from conical scanning: i.e. does wingbeat frequency provide an additional identification dimension that resolves target classes with similar size and shape?

The narrowness of the peak in the distribution of fundamental frequencies (Fig. 10a) suggests this character may be relatively useful for discriminating *C. terminifera* from other species with slightly lower or higher wingbeat rates. Many large migrant insects beat their wings at rates between 15 and 50 Hz (e.g. Riley et al., 1983; Reynolds and Riley, 1997), so the discriminating power may still not be high, but it should at least be possible to eliminate some alternative candidate species. The variation of the centre-frequency with height evident in Fig. 10(a) suggests that a correction for temperature (or possibly some other factor correlated with altitude) may significantly increase the diagnostic value of this character. The incidence rates of the second and third harmonics (Fig. 11) and their relative intensities (Fig. 12) appear to have potential as discriminating characters, as reasonable statistics can be accumulated over 1 night. The fixed interrogation geometry (from directly below) of IMR observations should minimise extrinsic sources of variation in these parameters, but account would have to be taken of any differences in the distributions of signal lengths when comparing samples.

The final parameter retrievable from stationary-beam observations that can help to identify the targets is the lower limit on the RCS. The appearance of a peak, albeit a relatively broad one, in the distribution of this quantity (Fig. 9) suggests that the size-range of a predominant target will be identifiable from the stationary-beam data, especially if results from the three polarisation angles used for these observations are examined separately. However, this information is potentially much less specific than the full parameterisation of the RCS polarisation pattern obtainable from the conical-scan observations and perhaps its only value is for confirming the inferred target size by a semi-independent and less complicated (and hence possibly more robust) method.

Counts and speed estimates are similar to those produced during conical-scan observations, provided echoes shorter than 0.8 s (the minimum duration for conical-scan analyses) are excluded from the counts. At present, stationary-beam counts and speeds are included in the automatically produced graphical presentations of IMR outputs (Drake et al., 2002), but are distinguished from the estimates derived from conical-scan data by showing them in a different colour. Differences between the counts from the two sources are to be expected (because of the slightly broader coverage when the beam is scanned and differing detection efficiencies for the two signal types), but calculation of a correction factor has not so far been attempted. Speed estimation from stationary-beam data relies on a value for the

beamwidth (which is well known) and is therefore perhaps more reliable than estimation from conical-scan observations, which also requires a value for the beam offset (which is quite difficult to determine precisely). At present, comparing speed estimates from the two methods appears to be the best way of calibrating the beam offset.

It is encouraging that although the migration on 11–12 February, 1999 was one of the most intense of the whole season, the success rate for analysing the echoes was still high. This indicates that the IMR is able to perform well, at least in its stationary-beam observing mode, when major migrations are underway. Inspection of the display output of the analysis algorithm for a small sample of echoes indicated that an improvement in the performance of the signal-selection and delimiting procedure at high target densities may be achievable and that an increase in the success rate would probably then follow. At low densities, the effectiveness of the stationary-beam mode, and of an IMR in general, will be limited by poor statistics, as very few targets then pass through the beam. The only really useful information that can be garnered in these circumstances is that migration is light and this is provided satisfactorily by either operating mode.

Acknowledgements

The IMR development and trials program has been supported technically by the workshop staff of the School of Physics and financially with grant support from the Australian Research Council.

Appendix A. Stationary-beam mode signal analysis

A.1. Nomenclature

a, b, c	quadratic, linear and constant terms in parabola (with subscript f denoting fitted values)
$a_0 \ldots a_3$	coefficients in Blackman–Harris window function (Nuttall, 1981, Eq. 23) $a_0 = 0.35875$, $a_1 = 0.48829$, $a_2 = 0.14128$, $a_3 = 0.01168$
C_R	radar calibration constant (W m^2)
f_s	digitisation sampling frequency (Hz)
f_c	Nyquist critical frequency (Hz)
g	quadratic coefficient in relation between s_{max} and p (dBm s^{-2})
G	antenna gain
h_k	Fourier transform input time series (RCS factors to power half)
H_l	Fourier transform output time series (RCS factors to power half)
I	power spectral density (or periodogram)
k	$8 \ln 2 = 5.545$, constant in Gaussian beamshape equation
N_s	length of selected time series

N_p	length of padded time series (input to Fourier transform)
p	distance (horizontal) of closest approach to beam axis (m)
p_{thr}	minimum value of p for signal to be analysable (m)
P	echo power at antenna (W)
$\mathrm{pr}(x)$	probability function for variable x
$\mathrm{Pr}(x)$	cumulative probability function for variable x (from lower limit of x)
r	perpendicular (horizontal) distance from beam axis (m)
R	range (i.e. altitude) (m)
s	signal intensity (corrected and scaled) (dBm)
s_{max}	peak value of s for an echo (dBm)
s_{thr}	minimum value of s for echo to be analysable (dBm)
s_0	maximum possible value of s_{max} (when $p = 0$) (dBm)
s_f	parabolic fit to signal (dBm)
s_m	modulation component of signal (dBm)
t	time (s)
t_c	time of closest approach (s)
t_0	arbitrary origin for time (start of sequence) (s)
v	speed (m s^{-1})
V	receiver output ('video') signal (V)
w	window function

Greek letters

δ	small time-dependent component of RCS modulation factor
Δ_f	frequency bin width (Hz)
ε_a, ε_s, ε_v	uncertainty (error) on quantity denoted by subscript
ϕ	azimuthal angle around beam axis (rad)
θ	polar angle out from beam axis (rad)
θ_F	beamwidth (full width at half power) (rad)
θ_Δ	beam axis offset for conical scan (rad)
μ	RCS modulation factor
σ	target radar cross section (RCS) (m^2)

A.2. Form of signal and parabolic fit

A circular parabolic reflector, evenly illuminated in azimuth, produces a beam that is symmetric about the antenna axis and has a main lobe with an approximately Gaussian shape (Probert-Jones, 1962),

$$G(\theta, \phi) = G_0 \exp(-k\theta^2/2\theta_F^2). \tag{A1}$$

This invariance with respect to azimuthal direction is maintained, at least to a good approximation, even when the transmission is linearly polarised along some direc-

tion ϕ_P: laboratory calibrations of an IMR antenna (Harman, unpublished data) show beamwidths in the electric- and magnetic-field directions differing by at most 5% out to distances from the axis corresponding to the 15-dB level for one-way transmission.

The power returned to the antenna after reflection from a target at altitude R is given by the radar equation (Skolnik 1980, pp. 3–4), which can be represented here in the simplified form

$$P_r(\theta) = C_R G^2(\theta)\sigma/R^4, \tag{A2}$$

where the constant C_R characterises the radar's sensitivity. The radar cross section σ will depend on both time (if the insect is wingbeating) and the insect's orientation ϕ_T relative to the beam polarisation ϕ_P, i.e. $\sigma = \sigma(\phi_T - \phi_P, t)$; however, the latter variation will only occur if the insect turns (yawing motion) as it traverses the beam. A target making a straight traverse of the beam at a steady speed v and with an unvarying alignment angle and passing at a distance of closest approach to the beam axis p at time t_c, will be located at distance

$$r(t) = \sqrt{v^2(t - t_c)^2 + p^2}. \tag{A3}$$

(Fig. 1c) after time t. Substituting Eq. (A1) into Eq. (A2) with $\theta = \theta(t) = r(t)/R$ from Eq. (A3), gives

$$\begin{aligned} P_r(t) &= C_R G_0^2 \exp(-kr^2/R^2\theta_F^2)\sigma/R^4 \\ &= C_R G_0^2[\exp(-kp^2/R^2\theta_F^2)/R^4]\exp(-kv^2(t - t_c)^2/R^2\theta_F^2)\sigma, \end{aligned} \tag{A4}$$

where all the terms before the second exponential function remain constant during the traverse.

The characteristic curve of the logarithmic receiver can be represented approximately as

$$V(t) = A\ \ln(P_r(t)) + B. \tag{A5}$$

There are, in fact, some minor deviations from an exactly logarithmic relationship (especially near the threshold of detectability). These can be measured in a receiver calibration and corrected for after digitisation, and as the calibration also estimates the radar constant C_R, the corrected values can be scaled to the conventional form of power relative to 1 mW, expressed in decibels (i.e. dBm). The net effect of these transformations is to calculate a 'video signal' $s(t)$ as

$$s(t) = 10 \log_{10}(P_r(t)) + 30. \tag{A6}$$

Applying this process to Eq. (A4), the signal from a traversing target will be of the form

$$s(t) = c(p, R) + a(v/R)(t - t_c)^2 + 10 \log_{10}\sigma(t), \tag{A7}$$

i.e. the sum of a quadratic in t and a term arising from the time dependence of the target's RCS.

The coefficients a and c are given by

$$c(p, R) = 10[\log_{10}(C_R G_0^2) + 3 - 4\log_{10}R - k\log_{10}e[p/R\theta_F]^2] \quad \text{(A8)}$$

and

$$a(v/R) = -10k\log_{10}e[v/R\theta_F]^2. \quad \text{(A9)}$$

Provided the target's orientation does not vary, modulation of the RCS will be due to changes in the shape of the target and for insects—where these changes arise principally from wingbeating—the time dependence of the last term in Eq. (A7) will usually be relatively small and appear as a ripple superimposed on the parabola (as in Figs. 4 and 5). (For birds, the modulation due to wingbeating is typically large (Konrad et al., 1968) and the parabolic shape may be obscured.) Estimates of the parabola parameters are obtained from the sequence of signal measurements s_i at times t_i by a generalised linear least-squares fit (Lyons, 1986) with the usual weighting $1/\varepsilon_{si}^2$, where ε_{si} is the estimated uncertainty (or 'measurement error') for measurement s_i. The ε_{si} have been set to a nominal 0.7 dBm, except at very low signal strengths where they are gradually increased to 2 dBm at the threshold for detection; these values are derived from the receiver calibration data and are compatible with residuals obtained in good quality fits to conical-scan echoes (Harman, unpublished data). Because the time of closest approach is unknown a priori, a full three-parameter parabolic fit is required; the outputs are the three coefficients in the fitted equation.

$$s_f(t) = a_f t^2 + b_f t + c_f, \quad \text{(A10)}$$

where t has its origin at the start of the measurement sequence.

A.3. Estimation of trajectory parameters

The quadratic parameter a_f from the fit can be substituted for a in Eq. (A9) to provide an estimate of the speed v

$$v = R\theta_F\sqrt{-a_f/10k\log_{10}e} = 0.2038R\theta_F\sqrt{-a_f}. \quad \text{(A11)}$$

The uncertainty (estimation error) on v is therefore (following e.g. Taylor, 1982)

$$\varepsilon_v = 0.2038R\theta_F\varepsilon_a/2\sqrt{-a_f} = -v\varepsilon_a/2a_f, \quad \text{(A12)}$$

where the uncertainty on a_f, ε_a, is an output from the least-squares fit. (For some applications, it may be appropriate to recognise additional uncertainty arising from the lack of precise knowledge of R, which is defined only by the 50-m length of the range gates, and possibly also from the uncertainty in the measurement of θ_F; if required, these terms can be estimated from the output results.)

The maximum signal value can be determined by first finding the time of closest approach, i.e. the time at which the parabola reaches its maximum,

$$t_c - t_0 = -b_f/2a_f, \tag{A13}$$

and then substituting this in Eq. (A10)

$$s_{max} = c_f - b_f^2/4a_f. \tag{A14}$$

This value can be equated to the sum of the first and third terms in Eq. (A7), but as there are two unknowns, p and $\sigma(t)$ and no additional information, neither can be determined. However, a lower limit on the RCS, σ_L, can be estimated by setting $p = 0$ in Eq. (A8) and substituting into Eq. (A7)

$$\log_{10} \sigma_L = (s_{max}/10) - \log_{10}(C_R G_0^2) - 3 + 4 \log_{10} R. \tag{A15}$$

This equation also describes a possible procedure for calibrating the radar: a target of known RCS is positioned on the beam axis at a known range, the signal produced by it is measured and an empirical value for $C_R G_0^2$ calculated.

A.4. Distribution of peak values

From Eq. (A7) and Eq. (A8) it can be seen that a population of identical targets at a particular range will produce signals with peak values s_{max} that depend on the distance of closest approach p as,

$$s_{max} = s_0 - gp^2, \tag{A16}$$

where

$$s_0 = 10[\log_{10}(C_R G_0^2) + 3 - 4 \log_{10} R + \log_{10} \sigma(t)] \tag{A17}$$

and

$$g = 10k \log_{10} e/(R\theta_F)^2. \tag{A18}$$

It is necessary to consider only targets that pass at or closer than the distance p_{thr} at which the target is just detectable,

$$p_{thr} = \sqrt{\frac{s_0 - s_{thr}}{g}}. \tag{A19}$$

As flights can be assumed to be unaffected by the radar, actual closest-approach distances, p', will be a uniformly distributed random variable,

$$\mathrm{pr}(p')\mathrm{d}p' = dp'/p_{thr}, \tag{A20}$$

where $0 \le p' \le p_{thr}$. The probability of a signal peaking at value s'$_{max}$ is given by

$$\mathrm{pr}(s'_{max})\mathrm{d}s'_{max} = \mathrm{pr}(p') \frac{\mathrm{d}p'}{\mathrm{d}s'_{max}} \mathrm{d}s'_{max} = \frac{1/p_{thr}}{-2gp'} \mathrm{d}s'_{max}, \tag{A21}$$

i.e.

$$\mathrm{pr}(s'_{max}) = \left| \frac{-1}{2p_{thr} g p'} \right| = \frac{1}{2\sqrt{(s_0 - s_{thr})(s_0 - s'_{max})}}. \tag{A22}$$

Here $s_{thr} \leq s'_{max} \leq s_0$. The negative signs in Eq. (A21) and Eq. (A22) reflect the decrease in s'_{max} with increasing p. This probability distribution is illustrated in Fig. 13, with parameters set to values appropriate for comparison with the distributions of Fig. 9(b). The distribution is strongly weighted towards values at and just below s_0: from the cumulative probability distribution

$$\Pr(s_{max}) = \int_{s_{thr}}^{s_{max}} \mathrm{pr}(s'_{max})\, \mathrm{d}s'_{max} = 1 - \sqrt{\frac{s_0 - s_{max}}{s_0 - s_{thr}}}, \tag{A23}$$

it can be seen that half the s'_{max} values occur in the topmost quarter of the s_0–s_{thr} range. This suggests that if a target population with a narrow distribution of RCS values passes over, a peak is still likely to be present in a plot of s_{max} values. This peak should have a relatively sharp upper cutoff from which a nominal s_0 value for the targets, and hence from Eq. (A17) a nominal RCS σ, can be estimated.

A.5. Analysis of modulation

The modulation of the RCS, $\sigma(t)$, produced by wingbeating can be represented by

$$\sigma(t) = \sigma_0 \mu(t), \tag{A24}$$

where σ_0 is the time-averaged RCS and the modulation factor $\mu(t)$ is always positive and averages to 1. If the modulation is small (as is generally the case for insects), then it may be useful to write

$$\mu(t) = 1 + \delta(t), \tag{A25}$$

where $\delta(t) \ll 1$ and time-averages to zero.

Writing Eq. (A7) as

$$s(t) = a(p, R) + c(v/R)(t - t_c)^2 + 10(\log_{10} \sigma_0 + \log_{10} \mu(t)), \tag{A7a}$$

it can be seen that after subtracting the parabolic fit (Eq. (A10)), the residual modulation is

$$s_m(t) = s(t) - s_f(t) = 10 \log_{10}(\mu(t)). \tag{A26}$$

As input to the Fourier transform, we estimate not $\mu(t)$ but its square root

$$h_l = \mu_l^{1/2}(t_l) = 10^{s_{ml}/20}. \tag{A27}$$

Here $l = 0, 1 \ldots N_s - 1$ is the index to the points in the time series, with $t_l = l/f_s$; s_{ml} is estimated from the lth signal digitisation using Eq. (A26) and Eq. (A10). To suppress low frequencies arising from the signal pedestal and leakage of spectral power into sidebands, the time series is modified by the usual processes of subtracting the mean and multiplying by a window function (Lyons, 1998a,b). The Blackman–Harris window, of form

$$w_l = a_0 - a_1 \cos(2l\pi/N_s) + a_2 \cos(4l\pi/N_s) - a_3 \cos(6l\pi/N_s), \tag{A28}$$

is used because of its extremely effective suppression of leakage sidelobes (Nuttall, 1981).

The definition of Fourier transform used is (Press et al., 1993)

$$H_m = \sum_{j=0}^{N_p-1} h_j w_j \exp(2\pi ijm/N_p) \quad m = 0,1\ldots N_p/2; \tag{A29}$$

here the mth component corresponds to frequency $f_m = m\Delta_f$, where $\Delta_f = f_s/N_p$ is the width of the frequency bins. The components h_j are set to zero for $N_s < j < N_p - 1$ ('zero padding'). The modified periodogram (or power spectrum), normalised to the series length N_s, is calculated from these H_m as

$$I(f_m) = I_m = \frac{2}{W}|H_m|^2, \tag{A30}$$

(with the factor 2 omitted when $m = 0$ or $N_p/2$), where

$$W = N_s \sum_{l=0}^{N_s-1} w_l^2, \tag{A31}$$

incorporates a weighting correction for the window function (Press et al., 1993). The periodogram intensities will scale as μ and thus (Eq. (A25) and Eq. (A2)) be proportional to both target RCS σ (cm^2) and received power P_r (mW).

The magnitude of the constant component (prior to subtraction of the mean, which invalidates the value from Eq. (A30)) can be calculated directly from the unweighted inputs as

$$I_0 = \frac{1}{N_s^2}\left|\sum_{N_s} h_l\right| = |\bar{h}|^2, \tag{A32}$$

and used to normalise the I_m values, which then represent the proportional modulation of the RCS at each frequency. As the h_l should average to 1 (Eq. (A24) and Eq. (A25)), this normalisation can, in practise, be omitted.

The frequency of a peak falling in bin n is estimated by the quadratic interpolation formula (Press et al., 1993),

$$f_p = \Delta_f\left(n + \frac{(P_{n+1} - P_{n-1})}{2(2P_n - P_{n+1} - P_{n-1})}\right). \tag{A33}$$

This formula is also used to estimate peak positions in the histograms presented in this paper.

References

Aldhous, A.C., 1989. An investigation of the polarization dependence of insect radar cross-sections at constant aspect. PhD thesis, Cranfield Institute of Technology, UK. 166 pp.

Drake, V.A., 1983. Collective orientation by nocturnally migrating Australian plague locusts, *Chortoicetes terminifera* (Walker) (Orthoptera: Acrididae): a radar study. Bull. Entomol. Res. 73, 679–692.

Drake, V.A., 1993. Insect-monitoring radar: a new source of information for migration research and operational pest forecasting. In: Corey, S.A., Dall, D.J., Milne, W.M. (Eds.), Pest Control and Sustainable Agriculture. CSIRO, Melbourne, pp. 452–455.

Drake, V.A., Farrow, R.A., 1983. The nocturnal migration of the Australian plague locust, *Chortoicetes terminifera* (Walker) (Orthoptera: Acrididae): quantitative radar observations of a series of northward flights. Bull. Entomol. Res. 73, 567–585.

Drake, V.A., Farrow, R.A., 1988. The influence of atmospheric structure and motions on insect migration. Ann. Rev. Entomol. 33, 183–210.

Drake, V.A., Gregg, P.C., Harman, I.T., Wang, H.K., Deveson, E.D., Hunter, D.M., Rochester, W.A., 2001. Characterizing insect migration systems in inland Australia with novel and traditional methodologies. In: Woiwod, I.P., Reynolds, D.R., Thomas, C.D. (Eds.), Insect Movement: Mechanisms and Consequences. CAB International, Wallingford, UK, pp. 207–233.

Drake, V.A., Wang, H.K., Harman, I.T., 2002. Insect Monitoring Radar: remote and network operation. Comput. Electron. Agric. 35, 77–94.

Dudley, R., 2000. The Biomechanics of Insect Flight. Princeton University Press, Princeton, NJ.

Konrad, T.G., Hicks, J.J., Dobson, E.B., 1968. Radar characteristics of birds in flight. Science 159, 274–280.

Lyons, L., 1986. Statistics for Nuclear and Particle Physicists. Cambridge University Press, Cambridge.

Lyons, R., 1998a. Windowing functions improve FFT results, Part I. Test and Measurement World, June 1998, pp. 37–44.

Lyons, R., 1998b. Windowing functions improve FFT results, Part II. Test and Measurement World, September 1998, pp. 53–60.

Nash, J.C., 1979. Compact Numerical Methods for Computers: Linear Algebra and Function Minimisation. Adam Hilger, Bristol.

Nuttall, A.H., 1981. Some windows with very good sidelobe behavior. IEEE Trans. Acoust. Speech Sign. Proc. ASSP 29, 84–91.

Press, W.H., Flannery, B.P., Teukolsky, S.A., Vetterling, W.T., 1993. Numerical Recipes in C: The Art of Scientific Computing, second ed. Cambridge University Press, Cambridge.

Probert-Jones, J.R., 1962. The radar equation in meteorology. Q. J. Roy. Meteorol. Soc. 88, 485–495.

Reynolds, D.R., Riley, J.R., 1997. Flight Behaviour and Migration of Insect Pests. Radar Studies in Developing Countries. NRI Bulletin 71. University of Greenwich, Chatham, UK.

Riley, J.R., 1985. Radar cross sections of insects. Proc. IEEE 73, 228–232.

Riley, J.R., Reynolds, D.R., 1979. Radar-based studies of the migratory flight of grasshoppers in the middle Niger area of Mali. Proc. R. Soc. Lond. B. 204, 67–82.

Riley, J.R., Reynolds, D.R., Farmery, M.J., 1983. Observations of the flight behaviour of the armyworm moth, *Spodoptera exempta*, at an emergence site using radar and infra-red optical techniques. Ecol. Entomol. 8, 395–418.

Schaefer, G.W., 1968. Bird recognition by radar. A study in quantitative radar ornithology. In: Murton, R.K., Wright, E.N. (Eds.), The Problems of Birds as Pests. Academic Press, London, pp. 53–86.

Schaefer, G.W., 1976. Radar observations of insect flight. In: Rainey, R.C. (Ed.), Insect Flight. Blackwell Scientific, Oxford, UK, pp. 157–197.

Simpson, R.E., 1987. Introductory Electronics for Scientists and Engineers, second ed. Allyn and Bacon, Newton, MA.

Skolnik, M.I., 1980. Introduction to Radar Systems, second ed. McGraw Hill, New York.

Smith, A.D., Riley, J.R., Gregory, R.D., 1993. A method for routine monitoring of the aerial migration of insects by using a vertical-looking radar. Phil. Trans. R. Soc. Lond. B. 340, 393–404.

Smith, A.D., Riley, J.R., Reynolds, D.R., 2000. The use of vertical-looking radar to continuously monitor the insect fauna flying at altitude over southern England. Bull. Entomol. Res. 90, 265–277.

Stroustrup, B., 1991. The C++ Programming Language, second ed. Addison-Wesley, Reading, MA.

Taylor, J.R., 1982. An Introduction to Error Analysis. University Science Books, Mill Valley, CA.